CFD SIMULATION OF CRITICAL HEAT FLUX IN A ROD BUNDLE

L. Vyskocil, J. Macek

Nuclear Research Institute Rez (NRI), Dept. of Thermal Hydraulic Analyses,
250 68 Rez, Czech Republic

Abstract
This paper presents CFD simulations of the boiling flow in a rod bundle with a Departure from Nucleate Boiling (DNB) condition at the end of the middle rod. "Large Water Loop" CHF experiments were used as a data set. The simulations were performed with multiphase code NEPTUNE_CFD V1.0.7. A simple criterion based on the void fraction at the wall was used for the CHF prediction.

Twenty one cases were selected from the data base and simulated on the coarse grid without grid spacers. The simulations were quite successful for cases with a low exit equilibrium quality. This method did not work for high exit equilibrium quality cases (X_{eq}>0.2). But these cases are most probably the dryout type of CHF while the numerical models were developed for DNB.

Several cases were calculated with simplified grid spacers in the computational domain. Modelling of the grid spacers leads to higher mixing and to a slightly lower calculated maximum void fraction. The results suggest that this modelling approach could be used for simulating the critical heat flux in the geometry of a reactor fuel assembly.

The presented work was carried out within the 7th FP EURATOM NURISP project. NEPTUNE_CFD code is implemented in the NURESIM platform.

1. INTRODUCTION

The critical heat flux (CHF) condition is characterized by a sharp reduction in the local heat transfer coefficient which results from replacing the liquid with vapour adjacent to the heat transfer surface. If the surface heat flux is the independent variable, the condition manifests itself as a sharp increase in the surface temperature as the critical heat flux value is reached. The critical heat flux forms an important boundary for the performance of the heat exchange equipment. Determining the critical heat flux is one of the key issues in nuclear reactor safety.

The goal of the work presented in this report was to assess the capability of NEPTUNE_CFD code to simulate the boiling flow with the critical heat flux in rod bundle geometry. NEPTUNE is a multiphase CFD code developed jointly by EDF R&D and CEA.

This report follows on the work presented in our companion paper submitted to this conference: Vyskocil, L., Macek, J.: "CFD Simulation of Critical Heat Flux in a Tube".

2. THE LARGE WATER LOOP EXPERIMENTAL FACILITY

The Large Water Loop (LWL) has been built at the Nuclear Machinery Plant, Skoda, Plzen Ltd., Czech Republic (see Bestion et al., 2006). The loop is non-active pressurised-water equipment with technological and thermal parameters corresponding to those of PWR.

The CHF experimental facility (part of the Large Water Loop) has been designed for research into CHF in water flow through a bundle of electrically heated vertical rods (nineteen rods, 9.1 mm diameter, 12.75 mm pitch). The heated length is 3.5 m. The critical conditions were determined under constant pressure, inlet water temperature and mass flux and for a quasi steady-state by gradually increasing the heat input.

The rods are modelled using hollow tubes with direct heating of the wall. The axial distribution of the wall heat flux is uniform while the radial distribution varies from a power coefficient of 1 for the central rod to 0.75 for the outer rods (see Fig. 1).

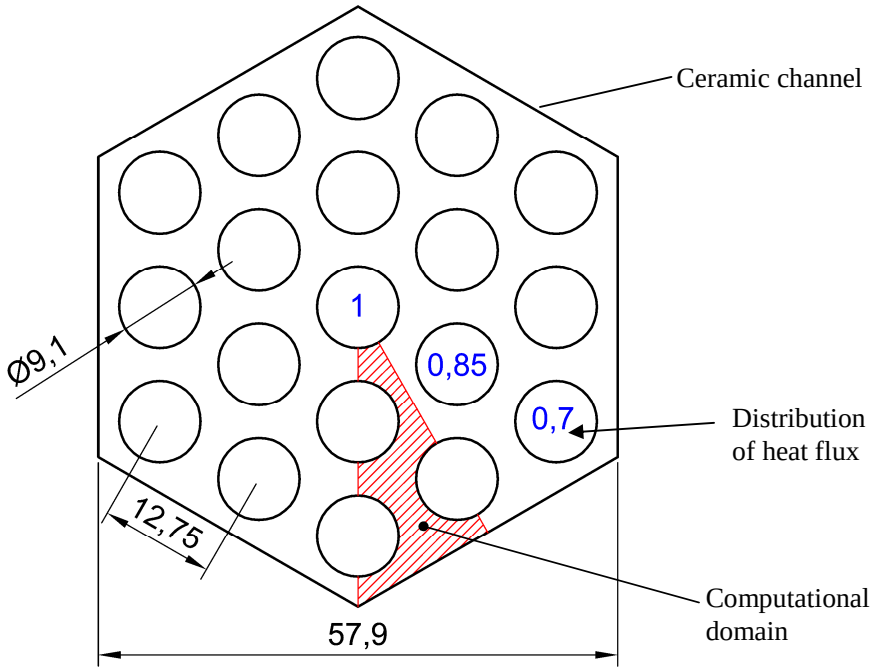

Fig. 1: LWL – Bundle D: horizontal cross section

3. MODELING BOILING FLOW UNDER CHF CONDITIONS

This chapter briefly presents the generalized boiling model, which is implemented in NEPTUNE code and used for numerical simulations of CHF in the rod bundle. The same model was previously used for simulations of CHF in tube geometry. A description of the sub-models (interfacial momentum, heat and mass transfer etc.) as well as the results of CHF simulations in the tube can be found in our companion paper submitted to this conference (Vyskocil and Macek, 2010).

The boiling model simulates the onset of nucleate boiling, partitioning of the wall heat flux and interfacial liquid-vapour heat, momentum and mass transfer. Two phases are modelled: the primary phase is liquid and the secondary is vapour bubbles. The same pressure is shared by the two phases. Continuity, momentum and energy equations are solved for each phase. The "k-ε liq" model (Yao, 2004) is used for modelling the liquid turbulence; the flow of vapour is assumed to be laminar. The distribution of the mean bubble diameter in the flow is modelled using a one-group interfacial area transport equation with models for bubble coalescence and breakup.

In order to account for a critical heat flux condition, the basic heat flux partitioning model by Kurul and Podowski (1990) was generalized as follows:

$$q_{wall} = f_{\alpha 1}\left(q_f + q_q + q_e\right) + \left(1 - f_{\alpha 1}\right) q_v \quad \left[W/m^2\right] \tag{1}$$

where q_{wall} is the total wall heat flux, q_f is the convective heat flux given to the liquid phase, q_q is the quenching part, q_e is the heat flux spent for liquid evaporation and q_v is the diffusive heat flux given to the vapour phase. $f_{\alpha 1}$ is the phenomenological function, which depends on the liquid volume fraction α_1 (Lavieville et al., 2005).

$$\alpha_1 > \alpha_{1,crit}: \quad f_{\alpha 1} = 1 - \frac{1}{2}\exp\left[-20\left(\alpha_1 - \alpha_{1,crit}\right)\right], \quad \alpha_{1,crit} = 0.2 \tag{2}$$

$$\alpha_1 < \alpha_{1,crit}: \quad f_{\alpha 1} = \frac{1}{2}\left(\frac{\alpha_1}{\alpha_{1,crit}}\right)^{20\alpha_{1,crit}} \tag{3}$$

The critical value for the void fraction is $1 - \alpha_{1,crit} = 0.8$. In our calculations, a local void fraction equal to 0.8 is used as a criterion for the CHF. Note that Weisman DNB criterion is a void fraction equal to 0.82 (Weisman, 1983).

4. SIMULATING CHF IN NEPTUNE

4.1 Computational Grid

The computational domain covers a 30° symmetric section of the actual channel (see Fig. 1). Only the 3.5 m long heated section is included in the domain. The cutting planes are modelled as a symmetry boundary condition. Four versions of the computational grid were created – see Fig. 2.

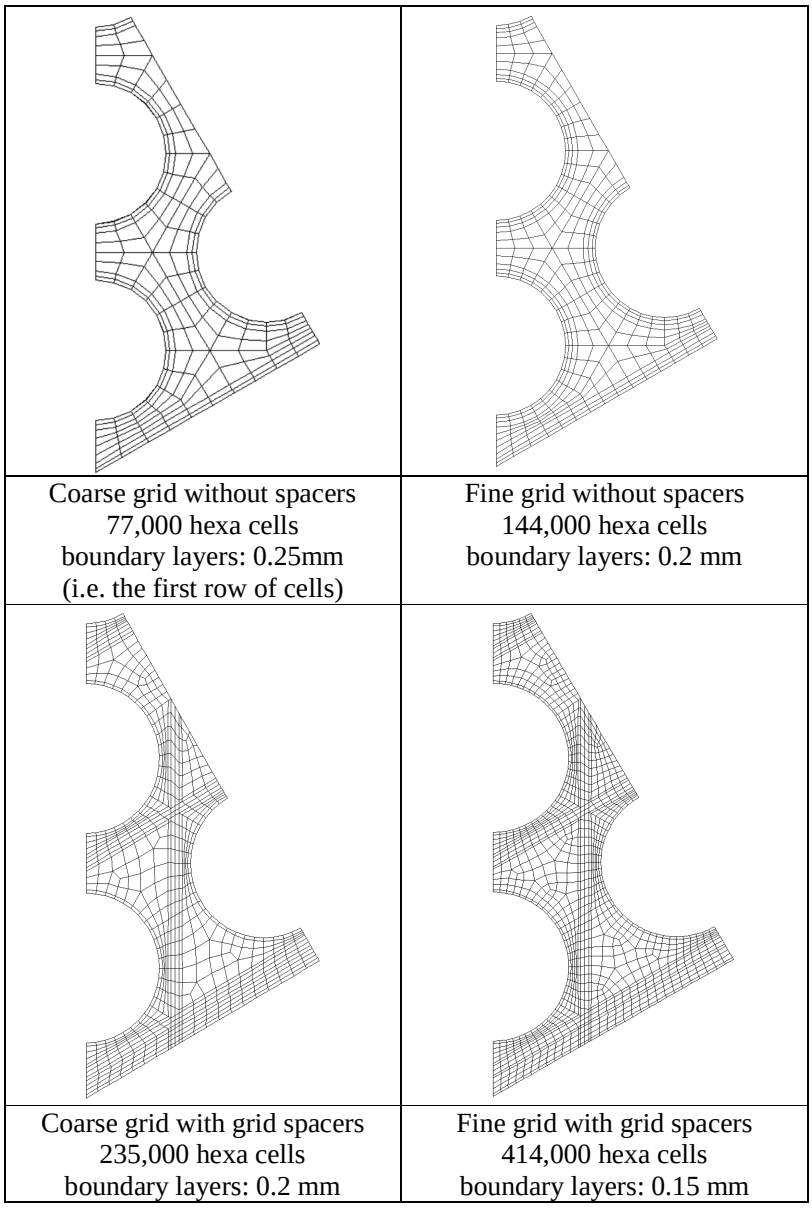

Fig. 2: Computational grids

A coarse grid without spacers was used to simulate all selected data points. A fine grid was used to test grid independence. Both grids have the same resolution in the axial direction.

The actual channel contains 7 grid spacers in the heated section – plates aligned with the flow. So as to assess the influence of the grid spacers on the results, several simulations were calculated on the coarse grid with simplified grid spacers. The actual grid spacers have braces that hold the rods in the correct position. These braces were omitted from the geometry so as to keep the total number of

cells within reasonable limits. A fine grid with spacers was then used to test grid independence. The shape of the simplified grid spacer is shown in Fig. 3.

4.2 Calculation Procedure

The actual experiments are quasi-steady. The inlet temperature, pressure and mass flux are constant and the wall heat fluxes are gradually increasing. The maximum temperature gradient is 2°C/min so the transients are too long to be calculated by NEPTUNE in a reasonable time. We decided to calculate the flow with steady boundary conditions (i.e. constant wall heat fluxes).

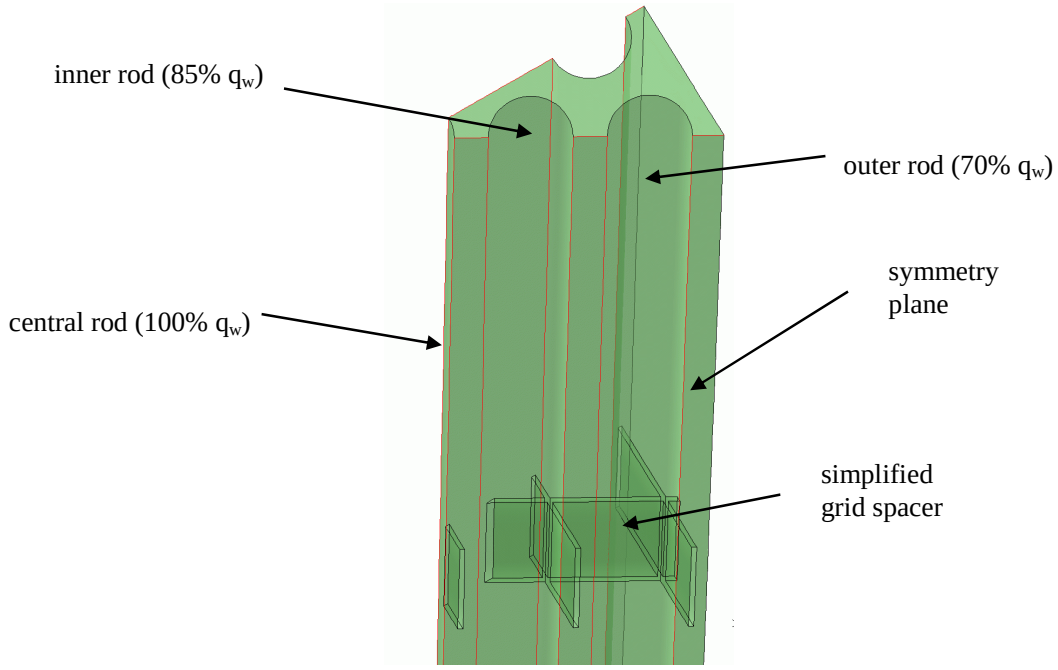

Fig. 3: Computational domain – exit part with simplified spacer grid

The calculations were performed with 100% wall heat fluxes right from the beginning. When the flow rate (liquid + vapour) leaving the domain was equal to the inlet flow rate and the wall temperatures and other parameters were stabilized, we analyzed the results. Depending on the results, the wall heat fluxes were decreased or increased so as to find the interval of the wall heat fluxes in which the maximum void fraction exceeds the critical value of 0.8.

5. TYPICAL RESULTS – SIMULATION WITHOUT GRID SPACERS

This chapter presents the results of a simulation of Test 67 on a mesh without grid spacers. The results of other cases are similar. The parameters of Test 67 are: pressure 11.962 MPa, inlet temperature 232.77 °C, mass flux 2054 kg/m^2/s, CHF 1.315 MW/m^2.

In this case, if 100% wall heat fluxes were used in the calculation, the calculated maximum void fraction exceeded the critical value of 0.8 (Fig. 4) and the central rod wall temperature started to increase at the end of the heated section (Fig. 6, see arrow). Decreasing the wall heat fluxes to 90% led to a decrease in the void fraction below the critical value (Fig. 5) and there was no increase in the wall temperature at the end of the heated section (Fig. 7).

The simulation of this case was successful, because the predicted CHF was between 90 – 100% of the experimental critical heat flux.

Note: the calculation domain in the following figures is vertically shrunk for visualization (scale 1:20). The actual height of the computational domain is 3.5 m and the diameter of the rods is 9.1 mm.

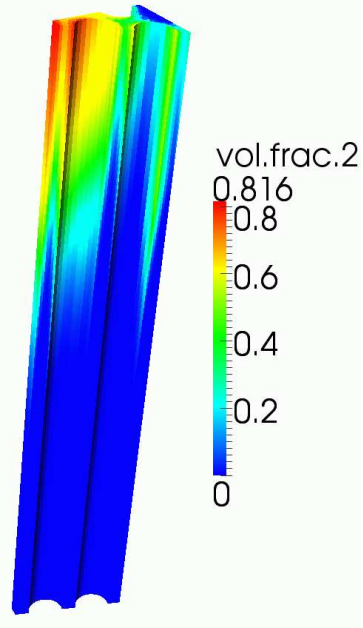

Fig. 4: Test 67: Void fraction [-], 100% wall heat fluxes, coarse mesh

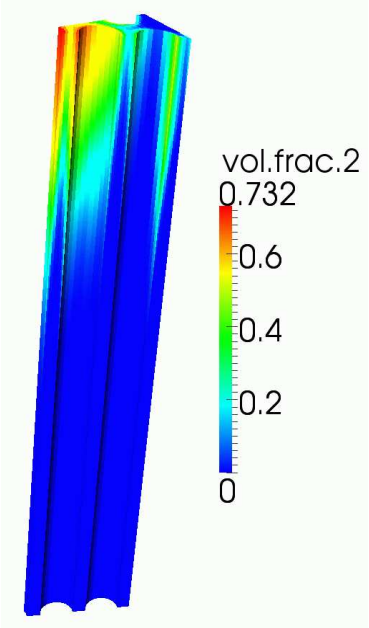

Fig. 5: Test 67: Void fraction [-], 90% wall heat fluxes, coarse mesh

100% wall heat fluxes: the wall heat fluxes used in the calculation were equal to those in the experiment.

90% wall heat fluxes: the distribution of heat fluxes was as follows – middle rod: 0.9·CHF, inner rods: 0.9·0.85·CHF, outer rods: 0.9·0.7·CHF

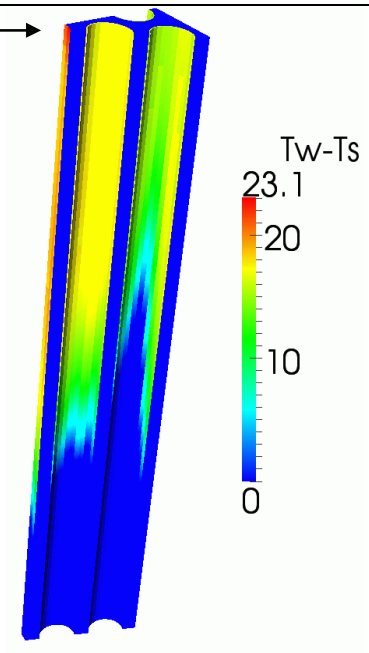

Fig. 6: Test 67: Wall superheating above saturation temperature [K], 100% wall heat fluxes, coarse mesh

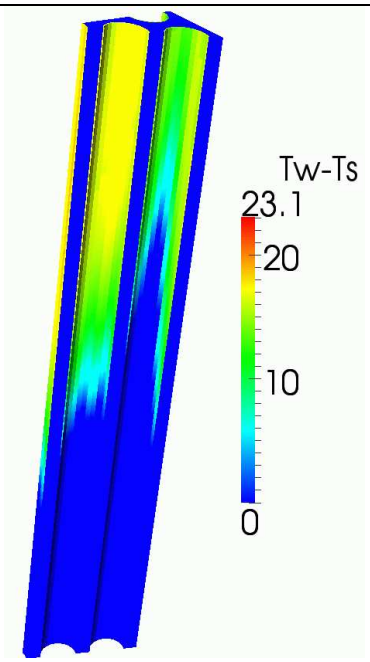

Fig. 7: Test 67: Wall superheating above saturation temperature [K], 90% wall heat fluxes, coarse mesh

The colour map range was clipped to an interval of < 0, max > in Fig. 6. Zero means that $T_{wall} \leq T_{sat}$. For clarity, both figures have the same range. The maximum superheating in Fig. 7 is 18.6 K.

5.1 Solution Grid Independence Test

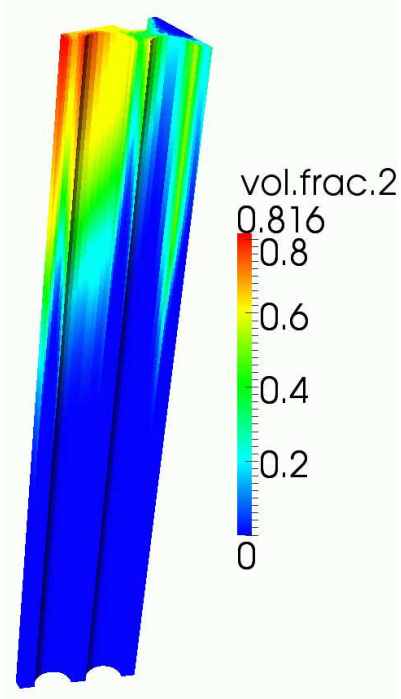

Fig. 8: Test 67: Void fraction [-], 100% wall heat fluxes, coarse mesh

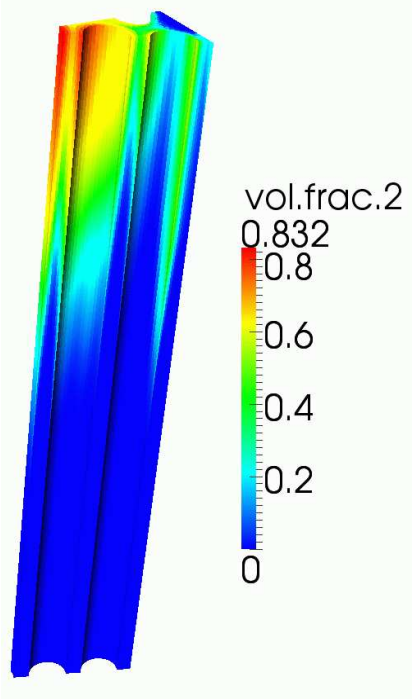

Fig. 9: Test 67: Void fraction [-], 100% wall heat fluxes, fine mesh

The same case was calculated on coarse mesh (77,000 cells) and fine mesh (144,000 cells). These meshes are displayed in Fig. 2. The above figures show a comparison of the calculated void fraction on coarse and fine mesh.

Table 1: Calculated maximum void fraction, Test 67:

	100% wall heat fluxes	90% wall heat fluxes
coarse mesh	0.816	0.732
fine mesh	0.832	0.752

It can be seen that the calculated void fraction distribution in the domain is almost the same on the coarse and fine mesh. The maximum void fraction is slightly higher on the fine mesh. CHF occurs between 90% and 100% of the experimental critical heat flux on both meshes.

6. SUMMARY OF RESULTS – SIMULATIONS WITHOUT GRID SPACERS

The following tables summarize the results obtained on the coarse mesh without grid spacers.

The calculation results with standard added mass force coefficient are not completely satisfactory in some cases; see for example Test 95 in Table 2. The use of added mass force coefficient by Zuber (1964) can improve the CHF prediction capability. On the other hand, the use of added mass force coefficient by Zuber leads to unstable solutions when the void fraction exceeds the critical value of 0.8. “Unstable” means that the calculation does not converge and “blows up”.

Table 2: LWL – summary of results – low exit equilibrium quality cases

Test No.	p_{out}	T_{in}	T_{sat}	G	CHF	X_{eq}	q_{calc}/CHF	α_{max}	α_{max}
	[MPa]	[°C]	[°C]	[kg/s/m^2]	[W/m^2]	[-]		standard AM	Zuber AM
3	14.091	284.88	337.18	1350	781922	0.174	100%	0.813	
							90%	0.76	0.99 n
							80%		0.706
68	11.927	249.94	324.21	2062	1180507	0.077	100%	0.806	0.96 n
							90%	0.733	0.779
80	10.317	237.45	313.30	2458	1403022	0.076	100%	0.847	
							90%	0.789	0.89 n
							80%		0.689
83	10.088	269.31	311.64	2937	1217940	0.097	100%	0.828	
							90%	0.778	0.93 n
							85%		0.788
							80%		0.712
87	16.098	151.22	347.85	979	1070983	-0.065	100%	0.711	0.702
							110%	0.781	0.99 n
							120%	0.863	
93	16.3	266.03	348.86	996	674477	0.096	100%	0.705	0.767
							110%	0.774	0.98 n
							120%	0.831	
112	13.858	300.41	335.86	4795	1646333	0.068	100%	0.681	
							110%	0.743	0.773
							120%	0.796	0.94 n
128	11.808	271.54	323.45	4274	1619992	0.029	100%	0.688	0.687
							110%	0.76	0.94 n
156	10.25	180.71	312.82	1548	1344101	0.080	100%	0.898	
							90%	0.836	0.96 n
							80%	0.716	0.71
157	10.347	181.42	313.52	2541	1894496	-0.003	100%	0.831	0.95 n
							95%		0.93 n
							90%	0.734	0.718
158	10.095	180.71	311.70	3523	2338833	-0.051	100%	0.751	0.779
							110%	0.901	0.95 n
160	14.109	182.29	337.28	1559	1315680	-0.061	100%	0.711	0.727
							110%	0.802	0.93 n
69	11.913	269.7	324.24	2070	1023153	0.101	100%	0.804	0.91 n
							90%	0.748	0.801
							80%		0.653
67	11.962	232.77	324.44	2054	1314987	0.058	100%	0.816	0.96 n
							90%	0.732	0.761
95	16.26	271.26	348.66	2060	1057812	-0.030	100%	0.557	
							110%	0.678	0.668
							120%	0.76	0.96 n
113	15.918	300.02	346.94	3798	1519479	0.039	100%	0.624	0.624
							110%		0.725
							120%	0.782	0.94 n

The predicted CHF in the low exit equilibrium quality cases (Table 2) is in the range of 80-120% of the experimental CHF if the added mass coefficient by Zuber is used.

The meaning of the symbols in the tables is as follows. p_{out} is the outlet pressure, T_{in} is the inlet temperature, T_{sat} is the saturation temperature, G is the mass flux. CHF is the experimental critical heat flux on the central rod and X_{eq} is the equilibrium exit quality calculated across the whole rod bundle. q_{calc} denotes the wall heat fluxes used in the calculation. For example, q_{calc}/CHF = 90% means that the heat fluxes used in the calculation were 0.9·CHF on the central rod, 0.9·0.85·CHF on the middle rod and 0.9·0.7·CHF on the outer rod (see the distribution of heat fluxes in Fig. 1). α_{max} is the calculated maximum void fraction.

Standard AM means that the standard added mass force coefficient c_{AM} = 0.5 was used in the calculation.
Zuber AM means that the added mass force coefficient by Zuber (1964) was used in the calculation:

$c_{AM} = 0.5\frac{1+2\alpha_v}{1-\alpha_v}$, α_v is the void fraction

Symbol "n" denotes an unstable solution.

Table 3: LWL – Results – high exit equilibrium quality cases

Test No.	p_{out}	T_{in}	T_{sat}	G	CHF	X_{eq}	q_{calc}/CHF	α_{max}	α_{max}
	[MPa]	[°C]	[°C]	[kg/s/m^2]	[W/m^2]	[-]		standard AM	Zuber AM
2	14.374	292.13	338.76	1236	725080	0.209	100%	0.826	
							90%	0.778	0.91 n
							80%		0.75
16	10.693	243.59	315.96	569	716068	0.554	60%	0.83	
							50%	0.71	
22	12.589	308.67	328.36	1225	625260	0.273	100%	0.904	
							90%	0.855	
							80%	0.814	
							70%	0.764	0.90 n
41	12.497	230.95	327.80	503	648135	0.516	75%	0.853	
							60%	0.675	0.799
155	9.922	182.66	310.42	518	798558	0.536	75%	0.897	
							60%	0.742	

The presented modelling approach does not work with high exit equilibrium quality cases (Table 3). But these cases are most probably dryouts while a generalized boiling model used in this work assumes a bubbly flow with a DNB-type of boiling crisis.

Unlike the simulations of CHF in the tube (Vyskocil, 2010), the CHF prediction method worked well for low pressure cases in the rod bundle (e.g. Test No. 83, 10.1 MPa) and low mass flux cases (e.g. Test No. 87, 979 kg/m^2/s). In simulations of CHF in pipes, oscillating solutions were obtained for low pressure cases. The results were not satisfactory in low mass flux cases in a tube.

7. SIMULATIONS WITH GRID SPACERS

Several cases were calculated with simplified grid spacers in the domain. The influence of the grid spacers on the results is shown in the following figures.

As expected, modelling the grid spacers leads to slightly higher mixing. The calculated maximum void fraction is lower than in the case without grid spacers. Note that the calculated maximum void fraction is below the CHF criterion in the case with grid spacers, however increasing the wall heat fluxes to 110% leads to a maximum void fraction of 0.849 which is above the CHF criterion.

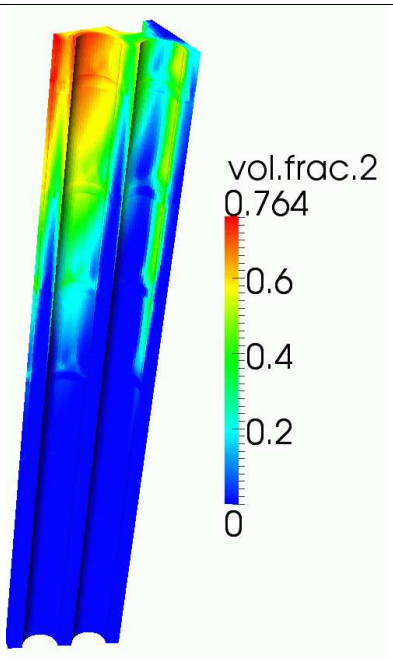

Fig. 10: Test 67: Void fraction [-], 100% wall heat fluxes, coarse mesh with grid spacers

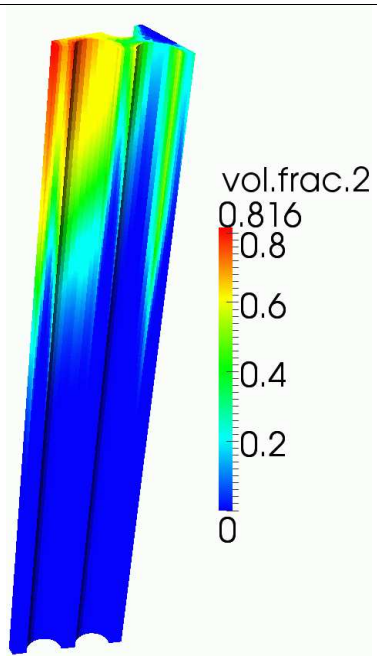

Fig. 11: Test 67: Void fraction [-], 100% wall heat fluxes, coarse mesh without grid spacers

Fig. 12 shows superheating of the wall above the saturation temperature when the wall heat fluxes were increased to 110% so as to create a CHF region in the calculation. The maximum void fraction is then 0.849. Note that there is a region with a sudden increase of wall temperature on the middle rod behind the last grid spacer (see arrow). The colour map range was clipped to an interval of < 0, 40K >. Zero means that $T_{wall} \leq T_{sat}$.

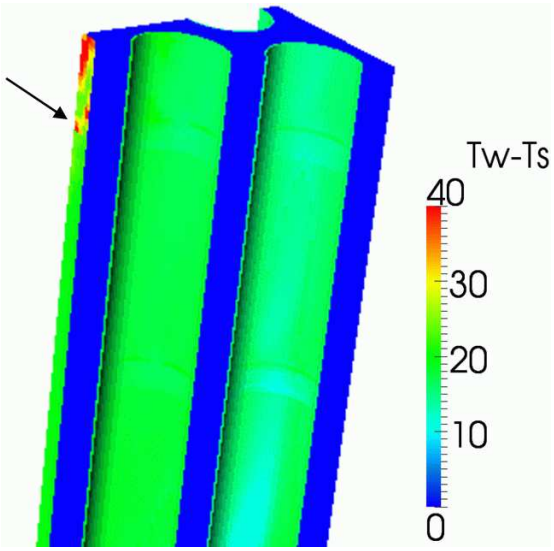

Fig. 12: Test 67: Wall superheating above saturation temperature [K], 110% wall heat fluxes, coarse mesh with grid spacers

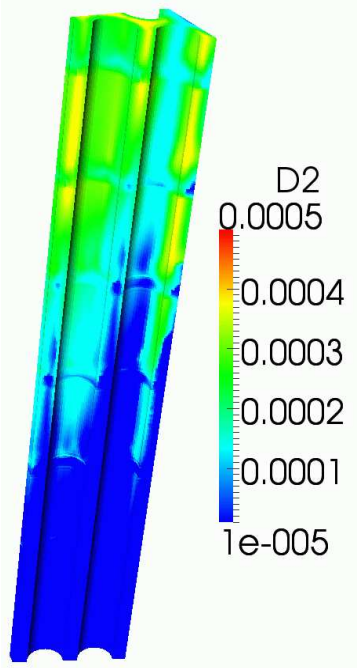

Fig. 13: Test 67: Mean bubble diameter [m], 100% wall heat fluxes, coarse mesh with grid spacers

Fig. 13 shows influence of grid spacers on the mean bubble diameter distribution. As the flow enters the grid spacer region, the bubbles break up. But just behind the grid spacer, the bubbles coalesce again.

Table 4 summarizes the results obtained with grid spacers in the computational domain.

Table 4: LWL – influence of grid spacers on the results

Test No.	p_{out}	T_{in}	T_{sat}	G	CHF	X_{eq}	grid	q_{calc}/CHF	α_{max}
	[MPa]	[°C]	[°C]	[kg/s/m^2]	[W/m^2]	[-]			std. AM
68	11.927	249.94	324.21	2062	1180507	0.077	coarse, no GS	100%	0.806
							coarse, GS	100%	0.774
112	13.858	300.41	335.86	4795	1646333	0.068	coarse, no GS	100%	0.681
							coarse, GS	100%	0.655
							coarse, no GS	110%	0.743
							coarse, GS	110%	0.725
67	11.962	232.77	324.44	2054	1314987	0.058	coarse, GS	110%	0.849
							coarse, no GS	100%	0.816
							coarse, GS	100%	0.764
							coarse, no GS	90%	0.732
2	14.374	292.13	338.76	1236	725080	0.209	coarse, no GS	100%	0.826
							coarse, GS	100%	0.826
							fine, no GS	100%	0.855
							fine, GS	100%	0.829
							coarse, no GS	90%	0.778
							coarse, GS	90%	0.775

GS = grid spacers

7.1 Solution Grid Independence Test

The same case was calculated on the coarse mesh with grid spacers (235,000 cells) and on the fine mesh with grid spacers (414,000 cells). These meshes are displayed in Fig. 2. The calculated void fraction distribution in the domain is almost the same on the coarse and the fine mesh (see Fig. 14 and Fig. 15).

The problem with the calculations with grid spacers is that the computational time drastically increases with the increasing complexity of the domain and the increasing total number of cells. Smaller cells in the domain require shorter time steps so as to fulfil Courant-Friedrichs-Lewy conditions. The calculation on the coarse mesh with grid spacers takes 8 days on 16 CPUs (Sgi Altix 350, 1400 MHz Itanium) while the calculation on fine mesh with grid spacers takes 32 days on 16 CPUs.

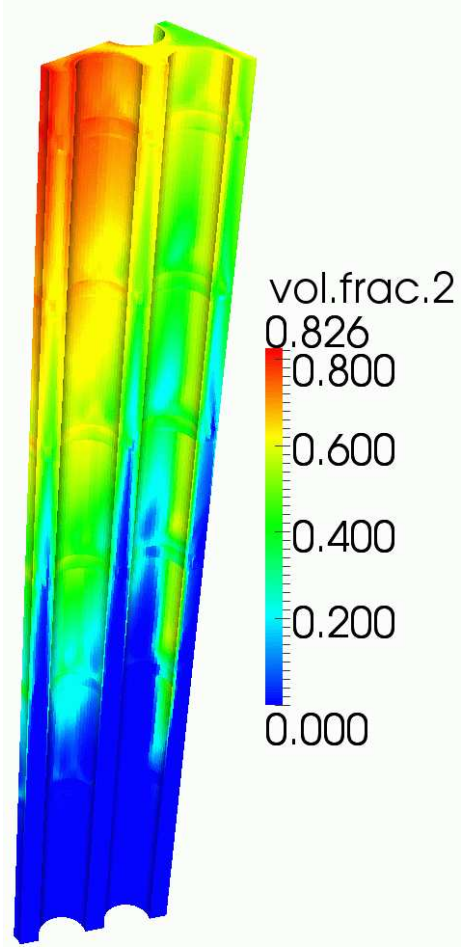

Fig. 14: Test 2, Void fraction [-], 100% wall heat fluxes, coarse mesh with grid spacers

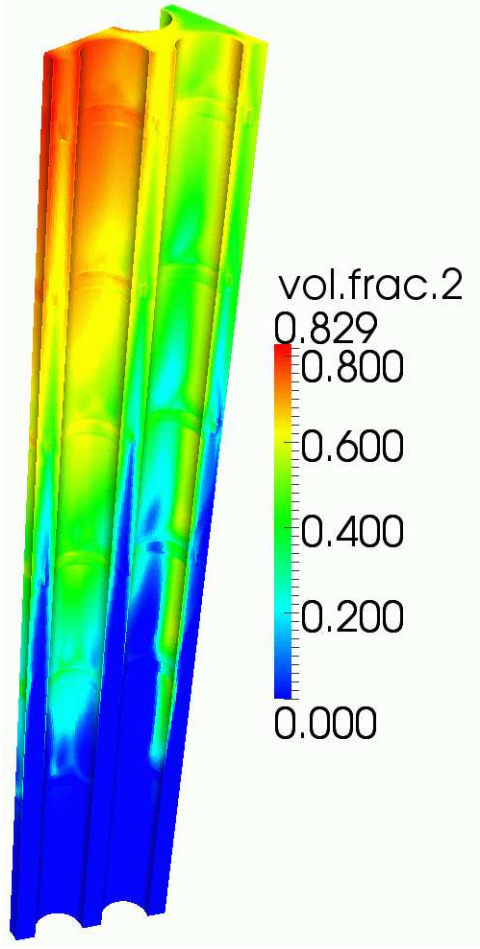

Fig. 15: Test 2, Void fraction [-], 100% wall heat fluxes, fine mesh with grid spacers

8. CONCLUSIONS

The capability of NEPTUNE_CFD code to simulate boiling flow with a critical heat flux in a bundle of heated vertical rods has been assessed. Large Water Loop CHF experiments were used as a data set. Twenty one cases were selected from the data base and simulated on coarse grid without grid spacers. The simulations were quite successful for cases with a low exit equilibrium quality. If the added mass coefficient by Zuber was used in the simulations, the predicted critical heat flux was within 80 - 120% of the experimental critical heat flux. Slightly worse results were obtained with the standard added mass coefficient.

On the other hand, this method did not work for high exit equilibrium quality cases ($X_{eq} > 0.2$). These cases are most probably a dryout type of CHF while the numerical models were developed for a DNB type of CHF.

Several cases were calculated with simplified grid spacers in the computational domain. Modelling the grid spacers leads to higher mixing and to slightly lower calculated maximum void fractions. The major problem encountered in the simulations with grid spacers is a significant increase in CPU time. The results suggest that this modelling approach could be used to simulate critical heat flux in the geometry of a reactor fuel assembly.

REFERENCES

Bestion, D., Caraghiaur, D., Anglart, H., Péturaud, P., Krepper, E., Prasser, H M., Lucas, D., Andreani M., Smith B., Mazzini D., Moretti F., Macek J.: "Deliverable D2.2.1: Review of the Existing Data Basis for the Validation of Models for CHF". *NURESIM-SP2 Deliverable* (2006)

Kurul, N., Podowski, M.Z.: "Multidimensional Effects in Forced Convection Subcooled Boiling", *Proceedings of the 9th International Heat Transfer Conference*, Jerusalem, Israel, 21-26 August (1990)

Lavieville, J., Quemerais, E., Mimouni, S., Boucker, M., Mechitoua, N.: "NEPTUNE CFD V1.0 Theory Manual", EDF (2005)

Vyskocil, L., Macek, J.: "CFD Simulation of Critical Heat Flux in a Tube", *CFD4NRS-3, OECD/NEA & IAEA Workshop*, Washington D.C., USA, 14–16 September (2010)

Weisman J., Pei, B.S.: "Prediction of Critical Heat Flux in Flow Boiling at Low Qualities", *Int. J. Heat Mass Transfer 26*, pp. 1463-1477 (1983)

Yao, W., Morel, C.: "Volumetric interfacial area prediction in upward bubbly two-phase flow", *Int. J. Heat and Mass Transfer* 47, pp. 307-328 (2004)

Zuber, N.: "On the dispersed two-phase flow in the laminar flow regime", *Chemical Engineering Science* 19, pp 897, 1964